

# Seasonal and Vertical Tidal Variability in the Southeastern Mediterranean Sea

Nadav Mantel<sup>1</sup>, Hezi Gildor<sup>2</sup>, Yizhak Feliks<sup>2</sup>, Pierre-Marie Poulain<sup>3</sup>, Elena Mauri<sup>4</sup>, and Milena Menna<sup>5</sup>

<sup>1</sup>Hebrew University of Jerusalem

<sup>2</sup>The Hebrew University

<sup>3</sup>OGS - Italy

<sup>4</sup>Istituto Nazionale di Oceanografia e di Geofisica Sperimentale (OGS), Italy

<sup>5</sup>National Institute of Oceanography and Applied Geophysics - OGS

September 30, 2023

## Abstract

Currents and pressure records from the DeepLev mooring station (Eastern Levantine Basin) are analyzed to identify the dominant tidal constituents and their seasonal and depth variability. Harmonic and spectral analysis on seasonal segments of currents and pressure reveal attributes of the tidal regime in the Eastern Levantine Basin: (1) Dominant semidiurnal sea-level variability; (2) seasonal variation of semidiurnal and diurnal tides found in both currents and pressure datasets; and (3) significant diurnal currents with weak semidiurnal currents in all seasons. The most dominant tidal constituent found from the pressure dataset is the M2 (12.4 h). Results from pressure datasets generally agree with previous models and observations of semidiurnal tides, while the diurnal tides are larger than previously reported by 8-9 cm in the winter and 1-2 cm in the summer. The surface current variability differs from the one reported before in the Eastern Levantine Basin, with M2 magnitudes weaker by 1 cm, while the diurnal tides (K1, O1) are 1-2 cm larger. Seasonal segments showed seasonal differences in the local tidal regime's amplitudes, with the K1 (7 cm difference between winter and fall) and S2 (4 cm difference between summer and fall) the most pronounced. We analyzed the M2 and S2 tides using surface drifters near DeepLev at different dataset lengths while considering the time constraints needed to resolve the tides adequately. The longer the dataset, the higher the resolution of the tidal analysis and the lower the amplitude leakages from nearby frequencies resulting in weaker tidal currents.

## Hosted file

973494\_0\_art\_file\_11396810\_s16p84.docx available at <https://authorea.com/users/663788/articles/667047-seasonal-and-vertical-tidal-variability-in-the-southeastern-mediterranean-sea>

## Hosted file

973494\_0\_supp\_11375259\_s0v4jd.docx available at <https://authorea.com/users/663788/articles/667047-seasonal-and-vertical-tidal-variability-in-the-southeastern-mediterranean-sea>

1  
2  
3  
4  
5  
6  
7  
8  
9  
10  
11  
12  
13  
14  
15  
16

## Seasonal and Vertical Tidal Variability in the Southeastern Mediterranean Sea

Nadav Mantel<sup>1</sup>, Yizhak Feliks<sup>1</sup>, Hezi Gildor<sup>1</sup>, Pierre-Marie Poulain<sup>2</sup>, Elena Mauri<sup>2</sup>, Milena Menna<sup>2</sup>

<sup>1</sup>The Institute of Earth Sciences, The Hebrew University of Jerusalem.

<sup>2</sup>Istituto Nazionale di Oceanografia e di Geofisica Sperimentale, OGS, Borgo Grotta Gigante, 42/c, 34010 Sgonico, Italy.

Corresponding author: Nadav Mantel ([nadav.mantel@mail.huji.ac.il](mailto:nadav.mantel@mail.huji.ac.il))

### Key Points:

- We analyze long-term measurements of velocity and pressure that enable seasonal and depth analysis of tides in the Eastern Levantine Basin
- The observed UPS1 apparently results from leakage of near-inertial motion
- Velocity from drifters and moored datasets were compared and used to assess different time criteria for tidal and spectral analysis

## 17 **Abstract**

18 Currents and pressure records from the DeepLev mooring station (Eastern Levantine Basin) are  
19 analyzed to identify the dominant tidal constituents and their seasonal and depth variability.  
20 Harmonic and spectral analysis on seasonal segments of currents and pressure reveal attributes of  
21 the tidal regime in the Eastern Levantine Basin: (1) Dominant semidiurnal sea-level variability;  
22 (2) seasonal variation of semidiurnal and diurnal tides found in both currents and pressure  
23 datasets; and (3) significant diurnal currents with weak semidiurnal currents in all seasons. The  
24 most dominant tidal constituent found from the pressure dataset is the M2 (12.4 h). Results from  
25 pressure datasets generally agree with previous models and observations of semidiurnal tides,  
26 while the diurnal tides are larger than previously reported by 8-9 cm in the winter and 1-2 cm in  
27 the summer. The surface current variability differs from the one reported before in the Eastern  
28 Levantine Basin, with M2 magnitudes weaker by 1 cm, while the diurnal tides (K1, O1) are 1-2  
29 cm larger. Seasonal segments showed seasonal differences in the local tidal regime's amplitudes,  
30 with the K1 (7 cm difference between winter and fall) and S2 (4 cm difference between summer  
31 and fall) the most pronounced. We analyzed the M2 and S2 tides using surface drifters near  
32 DeepLev at different dataset lengths while considering the time constraints needed to resolve the  
33 tides adequately. The longer the dataset, the higher the resolution of the tidal analysis and the  
34 lower the amplitude leakages from nearby frequencies resulting in weaker tidal currents.

35

## 36 **Plain Language Summary**

37 We examined the southeastern Mediterranean Sea tides, focusing on the Eastern Levantine  
38 Basin. Using data from a moored device located 50 km from the Israeli coast, recording pressure  
39 and currents from near surface to 1300 m depth and information from satellite-tracked surface  
40 drifters, we aimed to better understand tidal patterns in this region.

41 Our findings show (1) A prominent tidal elevation cycle occurring roughly every 12.4 hours. (2)  
42 Notable changes in tidal patterns across different seasons. For instance, the tides can be 8-9 cm  
43 higher in winter than in summer. (3) Significant daily tidal currents with weak twice-a-day  
44 currents in all seasons.

45 We noticed some differences when comparing data from fixed underwater devices and drifting  
46 ones. Drifters that collect data over longer periods give more detailed and accurate results.  
47 However, their movement across different areas can slightly alter the findings due to varying  
48 conditions.

49 Understanding these tidal patterns is crucial. It impacts several areas, from ensuring safer sea  
50 travel to understanding how pollutants spread in the water. Our study emphasizes the importance  
51 of using multiple data sources and considering time factors to comprehensively describe tidal  
52 variability.

## 53 **1 Introduction**

54 Tidal currents and tidal variations in sea level have attracted scholars for over 2000 years  
55 (see review by Deparis et al., 2013). Understanding tidal phenomena is essential for various  
56 practical applications, as these affect the dispersion of pollutants (Kar et al., 2022), larvae (Hsieh  
57 et al., 2010), the safety of marine transportation (Pastusiak, 2020), and more. In addition,  
58 numerical models are sensitive to the inclusion of tidal forcing (e.g., Naranjo et al., 2014;

59 Sannino et al., 2015). Tides in the Mediterranean Sea have been studied before, but only a few  
60 studies were conducted in the (deep part of the) Levantine Basin (summarized below). Here, we  
61 use long-term observations collected at the DeepLev mooring station in the Levantine Basin,  
62 hereinafter “DeepLev” (Katz et al., 2020), and satellite-tracked surface drifters to (1) identify the  
63 dominant tidal constituents in the Levantine Basin; (2) study the vertical and seasonal variability  
64 of the dominant constituents, and (3) compare the tidal constituents derived from moored current  
65 meters to those derived from surface drifters.

66

67 The Mediterranean is a semi-enclosed basin connected to the Atlantic Ocean by the  
68 Straits of Gibraltar, and it has a complex bathymetry. It is divided into two major basins by the  
69 Sicily Channel – the western basin and the eastern basin, and each basin includes many sub-  
70 basins, some shallow and some deep (Alberola et al., 1995; Gasparini et al., 2004). Thus, the  
71 characteristics of the tides can be different in different regions and depths (Poulain et al., 2018).

72

73 Tides in the Mediterranean were studied using both observations and models.  
74 Observations include current measurements from shipboard (Garcia-Gorriz et al., 2003;  
75 Gasparini et al., 2004), from moored instruments (Lafuente & Lucaya, 1994; Alb erola et al.,  
76 1995; Ursella et al., 2014), using high-frequency (HF) coastal radars (Chavanne et al., 2007;  
77 Cosoli et al., 2015; Soto-Navarro et al., 2016), and using surface drifters (Poulain et al., 2007,  
78 2013, 2015, 2018). In addition, numerical models with various complexities were also used to  
79 study tides in the Mediterranean Sea (e.g., Tsimplis et al., 1995; Arabelos et al., 2011).

80

81 A few previous studies identified four main constituents, M2, S2, K1, and O1 (e.g.,  
82 Gasparini et al., 2004; Tsimplis et al., 1995; Cosoli et al., 2015; S anchez-Rom an et al., 2018;  
83 Poulain et al., 2018), see Table 1 for the corresponding periods. Other studies identified and  
84 applied additional constituents in numerical models (Ferrarin et al., 2018; Arabelos et al., 2011).  
85 Differences in the dominant constituents at different locations are expected due to the complexity  
86 of the coastline and bathymetry.

87

88 There are specific constituents whose existence and importance need to be clarified,  
89 found in the tidal analysis, such as the diurnal UPS1 tide and the long fortnight Mf and Msf.  
90 Several observations at Alexandria have reported the presence of the UPS1 tide (El-Geziry &  
91 Radwan, 2012; El-Geziry, 2020; Khedr et al., 2018). 21.5-h oscillations, similar in the period to  
92 the UPS1 tide, were also observed at the Strait of Otranto (Ursella et al., 2014) and the Adriatic  
93 Sea (Medved et al., 2020). However, Ursula et al. (2014) and Medvedev et al. (2020) attributed  
94 this to the 21.5 h fundamental eigenmode in the Adriatic. At DeepLev, the inertial period is  
95 21.99 h, while the UPS1 tide is 21.4 h. Therefore, a time series of roughly 49.85 days is needed  
96 to separate the two signals in a spectral analysis. Not only is the inertial period near the UPS1 in  
97 all the Eastern Mediterranean with a period between 20.5 h to 23.05 h affecting diurnal  
98 frequency analysis, but there are also shifts in the effective inertial frequencies due to  
99 background vorticity (Perkins, 1976; Kunze, 1985). Therefore, the inertial band in the Eastern  
100 Mediterranean may be misinterpreted as the UPS1 tide by spectral and tidal analysis even with a  
101 longer time series than 49 days.

102

103 Studies at the Strait of Gibraltar identified the existence of the Mf and Msf constituents  
104 (Tsimplis & Bryden, 2000; Millot & Garcia-Lafuente, 2011; Sammartino et al., 2015). These  
105 frequencies could be attributed to non-linear interactions between semidiurnal and diurnal tidal  
106 constituents in shallow seas and sea shelves (Kwong et al., 1997). However, the Mf and Msf  
107 constituents have also been observed in the Adriatic Sea (Chavanne et al., 2007; Vilibić et al.,  
108 2015) and the Marmara Sea (Ferrarin et al., 2018), and our results of the Msf tide have shown to  
109 be significant in a few of the analyzed datasets.

110

111 The seasonality of tides, and in particular, the seasonality of the M2 tide, has been studied  
112 both theoretically and experimentally. Müller et al. (2014) showed variations in the M2 tide in  
113 global models and tide gauge data from several areas worldwide, such as Victoria, Canada, and  
114 Cuxhaven, Germany. Müller et al. (2014) attribute the effects of stratification to the seasonality  
115 of the tides with the view that stronger stratification leads to less mixing and, hence, to less loss  
116 of kinetic energy of the barotropic tide to turbulence. Wang et al. (2020) attempted to replicate  
117 the seasonality found in tide gauges in the Bohai Sea using a three-dimensional MITgcm model  
118 based on Müller's study with limited results. Ray (2022) proposes several physical mechanisms  
119 underlying the seasonality of the M2 tide group: climate-induced variations such as those found  
120 by Müller et al. (2014), astronomical changes due to the Sun's third-body perturbations of the  
121 lunar orbit, which are small, and compound tides such as the MSK2 tide. Ray (2022) used long-  
122 duration O(10 yrs) data sets taken from St. Malo (France), Chittagong (Bangladesh), and Port  
123 Orford (Oregon), which allowed the high-resolution spectral analysis necessary for such a study.  
124 Our study cannot capture the small frequency differences in the M2 tidal group, and we shall  
125 refer to them as the same constituent.

126

127 Drifters in the Eastern Levantine basin have also been used to study the tides in the  
128 region (Poulain et al., 2018). There are spatial and temporal limitations to using drifters for tidal  
129 analysis. Temporal constraints apply to the sampling frequency and period following signal  
130 analysis theory. More broadly, the confidence interval of the estimated values becomes narrower  
131 as the period increases (Bendat & Piersol, 1971). This phenomenon is experimentally shown in  
132 Lie et al. (2002), where longer, drifter datasets resulted in less deviation from the known M2 and  
133 K1 harmonic constants in the Yellow Sea. As for spatial limitations, when a drifter is transported  
134 hundreds of kilometers meridionally, the inertial frequency it experiences can vary significantly.  
135 As stated above, the inertial period is near the diurnal frequencies in the Eastern Mediterranean  
136 (specifically at DeepLev). Work on the M2 tide by Carrère et al. (2004) shows the M2's  
137 amplitude is not stable in areas where ocean mesoscale activities occur as well as areas with  
138 strong topographic features. The topography near the Israeli coast can change vastly, further  
139 affecting the tide, as seen in Rosentraub and Brenner (2007) through multiple moored devices  
140 along the coast. For these reasons, a maximal length of a dataset of the spatial order of  $1^\circ \times 1^\circ$  is  
141 needed to minimize the variability of the results due to spatial changes while keeping an accurate  
142 tidal harmonic analysis and spectral analysis.

143

144           Our results from pressure observations near the Israeli coast demonstrate a dominant M2  
145 tide constituent presence in every season and at all depths. In the current measurements, tidal  
146 analysis shows weak semi-diurnal and diurnal tides at all depths, with a seasonal difference  
147 between 3 cm/s in the fall and 0.9 cm/s in the spring for the tidal constituent of K1 at 30 m. In  
148 general, seasonality variations are less pronounced with depth. We also compared the tidal  
149 constituents' magnitudes derived from surface drifters to those derived from moored instruments.  
150 We demonstrated the difficulties associated with balancing the temporal length of the drifter's  
151 trajectory and its meridional movement.

152

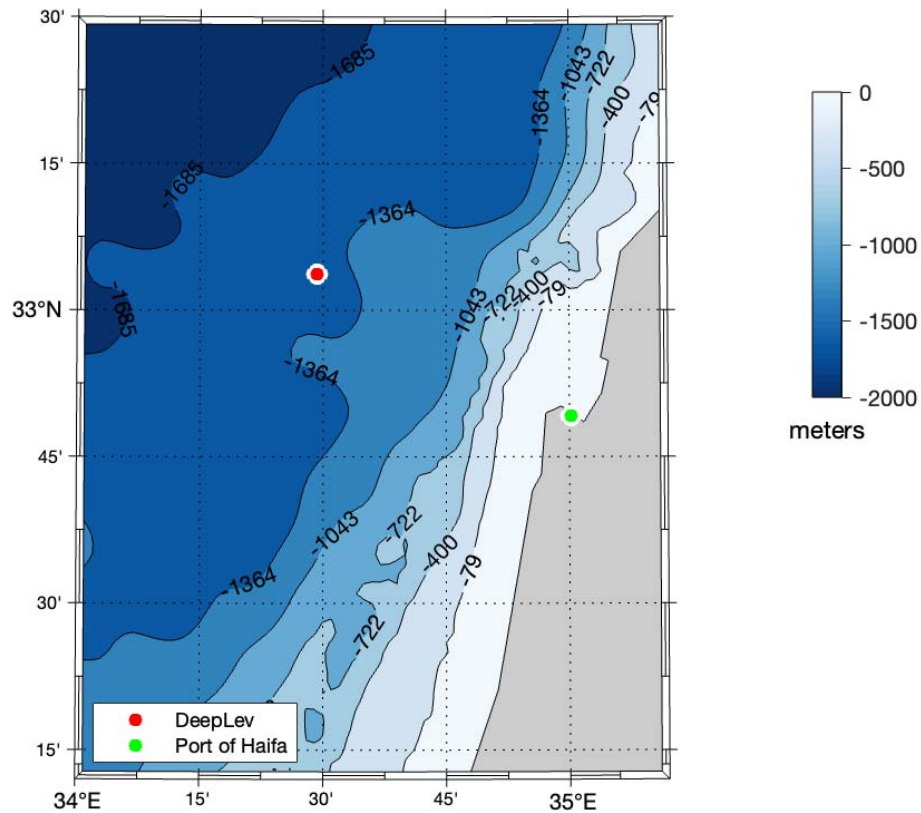
153           The paper's order is as follows: Section 2 describes the data used and analysis methods.  
154 In section 3, we present our results and conclude in section 4.

155 **2 Data and Methods**

156 The currents and pressure were measured at DeepLev (Fig. 1) ~50 km offshore Haifa,  
157 Israel, (33° 03.67' N; 34° 29.296' E), where the water depth is ~1500 m (Katz et al., 2020). The  
158 instruments were deployed for 6-9 months, with gaps in the data between consecutive  
159 deployments and occasionally within the deployment periods. For simplicity, we converted  
160 pressure from decibar to m using a 1:1 ratio for all the analyses presented in this paper. Table S1  
161 provides details on the analyzed time segments.

162

163 Currents were measured using Acoustic Doppler Current Profilers (ADCPS) employed at various  
164 depths. Three downward-looking Teledyne RDI ADCPs: One 300-kHz system was situated at  
165 approximately 30 m depth and measured from 30 m to 100 m in a 2 m bin, and formed  
166 ensembles every 15 min; A 150-kHz system was deployed at approximately 100 m, with 4 m bin  
167 size, formed an ensemble every 1 hr, down to about 200 m depth; Another 150-kHz system was  
168 at approximately 400 m and measured currents in 400-675 m, at 10 m bins and created  
169 ensembles every two h. Two Nortek Aquadopp single-point current meters were fixed at depths  
170 of 1310 m and 1492 m, measuring temperature, pressure, and currents, creating ensembles every  
171 ½ h. Five discrete depths were chosen from the measurements to analyze the current at different  
172 depths: 30 m, 50 m, 70 m, 160 m, 400 m, and 1300 m. These observed currents were used  
173 before to study intraseasonal variability (Feliks et al., 2022); here, we use the data to study the  
174 tides.



175

176 **Figure 1.** The location of the DeepLev mooring station (white full circle with a red dot), the  
 177 location of the Port of Haifa (white circle with a red dot), with bathymetry contour color.

178 Pressure variability was recorded by two RBR-CONCERTO CTDs placed at 80 m and 290 m  
 179 depths, measuring at a time resolution of 10 min in the first deployment and one min in the  
 180 following deployments. A SeaBird MicroCat CTD, placed at 185 m, was added to the array  
 181 starting deployment two with a time resolution of 10 min throughout. CTD depths are noted as  
 182 80 m, 200 m, and 300 m. Additional pressure measurements were used from the Nortek  
 183 Aquadopp at 1310 m, noted as 1300 m.

184

185 To analyze the M2 and S2 tides, which have a difference of 0.0028 cycles per hour, a minimum  
 186 of 15-day hourly data is required to separate the frequencies in a spectral analysis based on the  
 187 Rayleigh criterion  $\Delta f = 1/T$  using an unsmoothed periodogram or a rectangular window. For  
 188 smoothed periodograms or other windows, such as the ones used here, even longer data sets are  
 189 required (for more details regarding the Rayleigh criterion, see Thomson & Emery (2014)).  
 190 However, the criterion will produce peaks that are "just resolved"; this period length is not long  
 191 enough to ensure no leakage between the two frequencies. "Well-resolved" peaks have a  
 192 criterion  $\Delta f > 3/2T$  for unsmoothed periodograms. Here, we compare the common 15-day data

193 length set with longer data sets of 22.15-day (hereafter referred to as 22-day) or 30-day to  
194 evaluate the impact of spectral leakage on instrumental data.

195

196 The comparison is made in Section 3.2.2 using data from the first 60 days of the four seasons  
197 from 2017. Only 60 days were taken in the analysis since there are gaps between deployments in  
198 2017, giving two seasons with less than 90 days to compare the 15-day, 22-day, and 30-day  
199 analyses. For the 15-day analysis, a season was split by taking the first four 15-day segments  
200 with no overlap. After the tidal harmonic analysis, the magnitudes were averaged to give one  
201 result for the 15-day segment. For the 22-day analysis, the same season was split into the first  
202 three 22-day segments with no overlap. After the tidal harmonic analysis, the magnitudes were  
203 averaged to give one result for the 22-day segment. For the 30-day analysis, the same season was  
204 split into the first two 30-day segments with no overlap. After the tidal harmonic analysis, the  
205 magnitudes were averaged to give one result for the 30-day segment. All analyses were done for  
206 three different depths of 70 m, 160 m, and 1300 m.

207

208 Section 3.3 also used the trajectories of surface drifters deployed along the Israeli coast. The  
209 drifters used were the Surface Velocity Programme SVP drifter design with a drogue centered at  
210 15 m depth, manufactured by METOCEAN. Each drifter provides its location through the global  
211 positioning system (GPS) and transmits the data on land via the Iridium satellite link. The drifter  
212 position time series were first edited from spike and outliers, then linearly interpolated at regular  
213 0.5-h intervals using the kriging technique (optimal interpolation; Hansen & Poulain, 1996).  
214 Velocity components were then estimated from centered finite differences of 0.5-h sub-sampled  
215 positions (Menna et al., 2018).

216

217 We analyzed periods of 15-day with 50% overlap, 22-day with 50% overlap, and 30-day with  
218 50% overlap where drifters were within  $1^\circ$  of DeepLev. The locations of the drifters (in Latitude-  
219 Longitude coordinates) were converted to velocities using a first central difference algorithm  
220 from the MATLAB package by Lilly (2021). We split the drifter data into segments of 15, 22,  
221 and 30-day to study the M2 and S2 tides. The current data from DeepLev, analyzed in section 3.3  
222 as a comparison with drifter data, was taken from 50 m depth due to the lack of continuous data  
223 at shallower depths for most of the drifters' deployments. Only during the first deployment was  
224 their data at around 10 m. Matlab's corr function calculated the correlation coefficient between  
225 the 10 m, 30 m, and 50 m u (eastward velocity) and v (northward velocity) data above 0.89 with  
226 a p-value of practically null.

227

228 The choice of the bin size of  $1^\circ$  from DeepLev is based on the work done by Carrère et al. (2014)  
229 on the global stability of the M2 tide. Focusing on semidiurnal tides arises from the  
230 "contamination" by near-inertial oscillations and diurnal breeze (Poulain et al., 2018) on the  
231 diurnal tides. There were 32 segments of 15-day from 14 different drifters covering the seasons  
232 of 2017 and the summer of 2018. Of these segments, four were in the winter, 10 in the spring, 15

233 in the summer, and three in the fall. There were 12 segments of 22-day from 5 drifters. Of these  
234 segments, one was in the winter, six in the spring, four in the summer, and one in the fall. There  
235 were seven segments of 30-day from 3 drifters covering the spring and summer of 2017 and one  
236 remaining in the spring of 2018.

237

238 Tidal harmonic analysis was done using the `t_tide` MATLAB package (Pawlowicz & Lentz,  
239 2002). The magnitude of the current signal was computed by taking the square root of the  
240 amplitudes of semi-major and semi-minor axes. Amplitudes and corresponding Signal-to-noise  
241 (SNR) were estimated using a linearized error analysis that assumes a red noise model  
242 (Pawlowicz & Lentz, 2002). All tidal constituents' amplitude and inclination following will be  
243 those found to have an SNR of above 1. Hereinafter, we will refer to the magnitudes of the  
244 current signal as magnitude and the amplitudes of the pressure variability signal as amplitudes.  
245 The average magnitudes and amplitudes were calculated only concerning results with an SNR  
246 above 1; the rest were labeled Not Significant (N/S). The toolbox gives the explained variance of  
247 the significant tidal signal.

248

249 We also conducted spectral analysis (Power Spectral Density, PSD) using a multitaper method  
250 introduced by Thomson (1982) and further utilized in a MATLAB package by Lilly (2021). In  
251 this analysis, the PSD graphs are rotary spectra of the currents and the real-valued time series for  
252 the pressure. Four Slepian tapers were used for the rotary spectra, while for the pressure, one  
253 Slepian taper was used (Slepian, 1978). Significance levels of 95% were calculated using the  
254 signal's red noise spectra as the null hypothesis and F-test statistics to find the 95% significance  
255 levels. The degrees of freedom (DOF) are calculated  $K = 2P - 1$  where  $K$  is the DOF, and  $P$  is the  
256 number of Slepian tapers used in the analysis. We used this assuming that singly tapered spectral  
257 estimates follow a scaled chi-squared ( $\chi^2$ ) distribution (Percival & Walden, 1998).

258

259 All the samples have been split by season, defined as winter (December-February); spring  
260 (March-May); summer (June-August); and autumn (September-November). A description of the  
261 exact durations is presented in Table S1. Due to the nature of the study into diurnal and  
262 semidiurnal tidal constituents, a required resolution of 0.001 cycles per hour is needed to  
263 differentiate between the tides, detailed in Table 1, and various tidal constituents in their spectral  
264 vicinity. This limitation excludes any sample shorter than 30 days, except for the drifter analysis.  
265 Segments were also cut by a restriction of a maximal gap of 3 hours between credible data points  
266 (credible as defined by Katz et al., 2020). If a segment has two parts with a gap larger than 3  
267 hours in between, the longer segment was used to represent the season. For gaps shorter than 3  
268 hours, a linear interpolation was used. After interpolation, a linear detrend was performed.

269

270 The 400 m depth data is sampled every 2 hours, and this sampling cannot use the linearized error  
271 analysis offered by the `T_Tide` library, which requires a maximum delta of 1 hour. For this data  
272 set, we used a white random noise error analysis offered by the `T_Tide` library, which has a

273 slightly less conservative SNR than the linearized error analysis. Even with this difference, the  
 274 analyzed data from the 400 m data set did not differ substantially from the other analyzed data  
 275 sets. To further compare our results from DeepLev, we used the OSU TPXO model (Egbert &  
 276 Erofeeva, 2002) positioned at the location of DeepLev (33° 03.67' N; 34° 29.296' E).

277

Tide	Period
Primary tides of the study	
S2	12 hr
M2	12.4 hr
K1	23.9 hr
O1	25.8 hr
Other tides mentioned in the study	
UPS1	21.5 hr
Mf	13.66-day
Msf	14.8-day

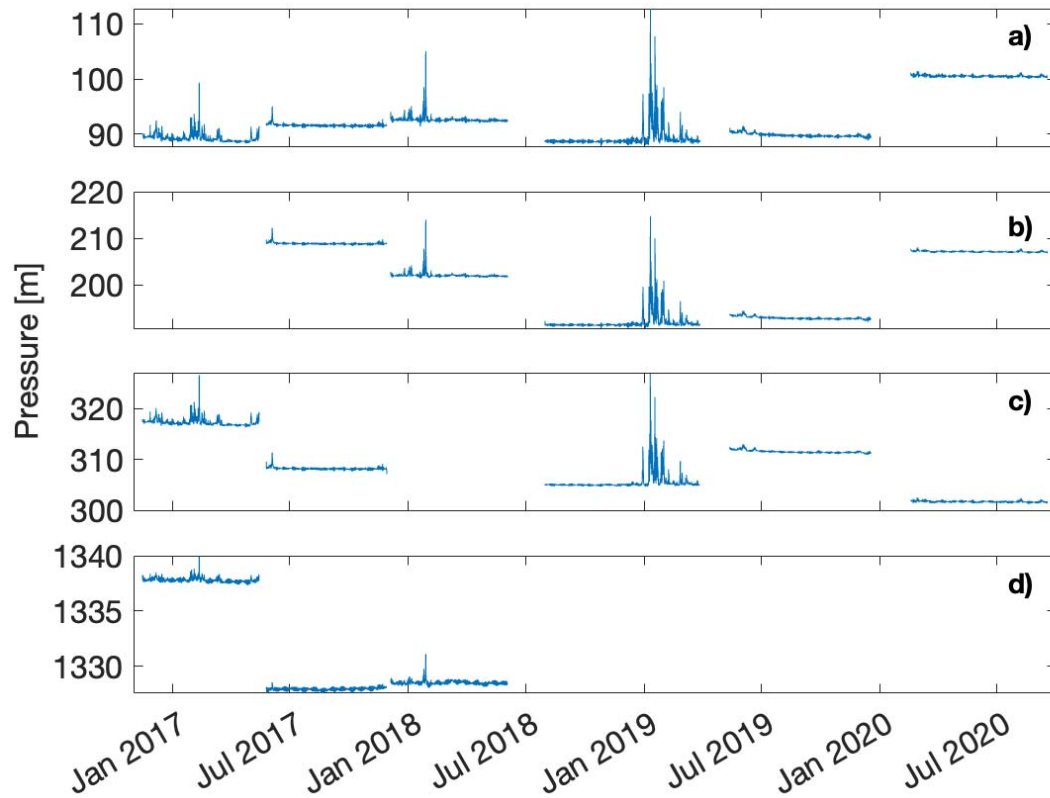
278 **Table 1.** Tidal constituents and their periods are either the primary focus or are mentioned in this  
 279 paper.

## 280 **3 Results**

### 281 **3.1 Pressure Variability**

282 CTDs at depths of around 90 m, 200 m, 300 m, and 1300 m recorded pressure during six  
 283 deployment periods between 11/2016 and 11/ 2020. Except during winter, most records show a  
 284 1-2 m variability. The winters show a much higher variability, reaching levels over 20 m, as seen  
 285 in Jan 2019 (Fig. 2).

286

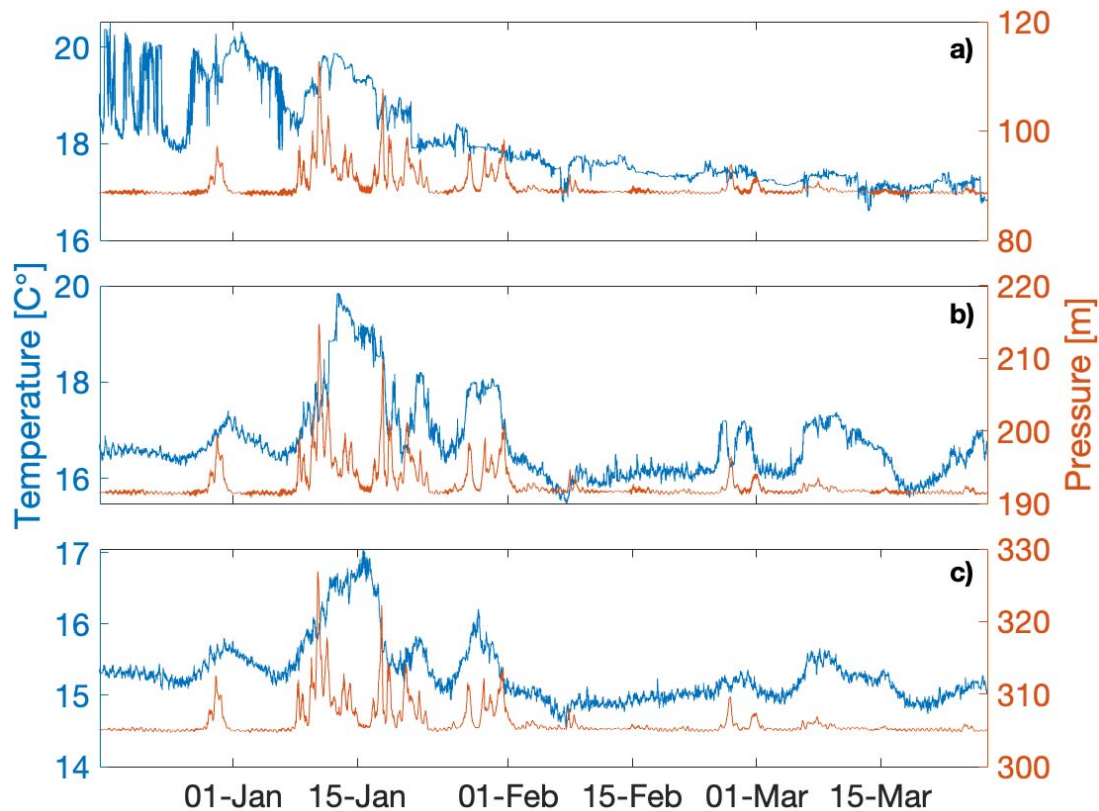


287 **Figure 2.** Pressure time series, measured in m, at four depths measured: (a) 90 m, (b) 200 m, (c)  
 288 300 m, and (d) 1300 m. Measurements started in November 2016 and ended in June 2020. There  
 289 were no measurements for all the depths, as described in Table S1. Each deployment was  
 290 measured at a slightly different depth, which is the reason for the differences in pressure between  
 291 deployment periods.

292

293 The large fluctuations in the winter, specifically in Jan 2019, might be due to a tilting of the  
 294 mooring device from strong horizontal motions (Katz et al., 2020). The currents could result  
 295 from a mesoscale eddy passing in the area of DeepLev. As shown in Feliks and Itzikowitz  
 296 (1987), the characteristics of eddies in the Eastern Mediterranean can bring changes and  
 297 displacements in temperature and pressure of around 20 m at depths down to 300 m. A study of  
 298 the temperature changes, shown in Fig. 3 around January 2019, shows similar results to those  
 299 that characterize an eddy in the Eastern Mediterranean. Synoptic maps (not shown) of pressure  
 300 from NCEP reanalysis in January do not display any storm in the area. In general, along with the  
 301 tides, strong horizontal currents may tilt the mooring devices, creating motions that may be  
 302 interpreted as vertical perturbations. To move the devices vertically 22 m, the approximate  
 303 maximum vertical variation in Fig. 3, the tilt needed is approximately 10.5 degrees, giving a  
 304 horizontal deviation of 236.9 m.

305



306 **Figure 3.** Temperature and pressure time series, measured in degrees Celsius and m, at three  
 307 depths measured: (a) 90 m, (b) 200 m, and (c) 300 m between 17/12/18 and 27/3/19.

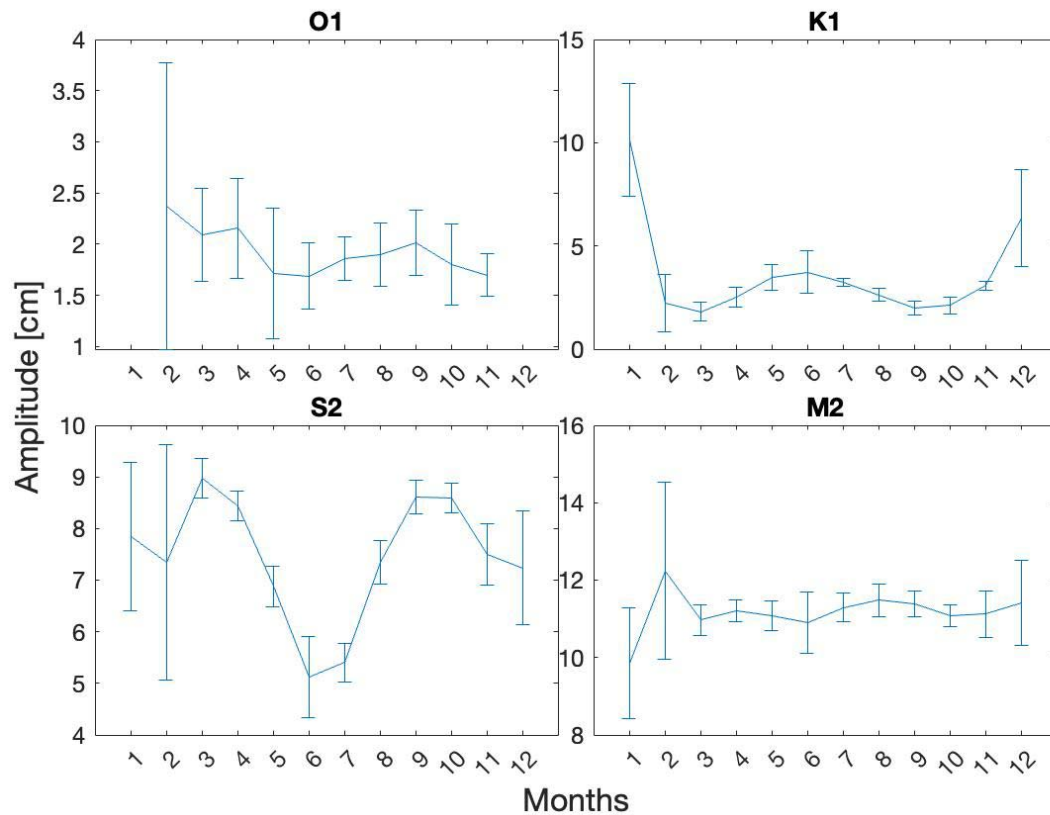
### 308 3.1.1 Tidal Analysis of Pressure Variability

309 Several tidal constituents are evident in the pressure variability. The foremost semidiurnal and  
 310 diurnal tides, S2, M2, K1, and O1, vary slightly between years and depths (Table S2 in the  
 311 appendix), demonstrating the barotropic characteristics. This agrees with several models  
 312 calibrated with experimental results (Tsimplis et al., 1995; Arabelos et al., 2011) and a time  
 313 series in the Western Mediterranean (Alberola et al., 1995).

314

315 The amplitude of M2 is the most dominant. It varies with time and depth between 9.5-12 cm, in  
 316 good agreement with tide gauges (Tsimplis et al., 1995), models (Tsimplis et al., 1995; Arabelos  
 317 et al., 2011) as well as the OSU TPXO barotropic model (Egbert & Erofeeva, 2002) with an  
 318 amplitude of 10.7 cm. The M2 amplitude is consistent, with no evident seasonal or depth  
 319 variability. The S2 amplitude ranges between 5.6-8.3 cm, with no depth variability but with  
 320 seasonal variability, as seen in Fig. 4, with fall averaging 8.2 cm and summer averaging 6.1 cm.  
 321 The results from previous studies (Tsimplis et al., 1995; Arabelos et al., 2011) show a range of 7-  
 322 8 cm, and the OSU TPXO shows 6.2 cm. O1 ranges between 2-3 cm, with few singular  
 323 exceptional amplitudes of 10 cm found in all depths of winter 2017, larger than the previously

324 observed and modeled results of 1-2 cm and the OSU TPXO showing 1.9 cm. The K1 tide varies  
 325 with season, with larger amplitudes in winter (~10 cm) at 90 m depth and summer amplitudes in  
 326 the 2.5-3.5 cm range. The significant differences between seasons in K1 are smaller at 1300 m  
 327 with amplitudes of 3.5-4 cm in the winter and 2.5-3 cm in the summer. These results are also  
 328 larger than predicted or recorded in previous studies of 1-2 cm, and the OSU TPXO shows 1.7  
 329 cm. The changes in depth can be attributed to the leakage of atmospheric stress to the diurnal  
 330 bands. The O1 and K1 are anomalously high in the winter, significantly larger than previously  
 331 observed. A possible explanation for the heightened amplitude is the leakage of the inertial  
 332 period into the diurnal frequencies due to winter eddies near DeepLev, such as the one  
 333 showcased in section 3.1.



334

335 **Figure 4.** The average monthly amplitudes [cm] of the four major tides analyzed from the 2017-  
 336 2020 pressure time series at 200 m depth. The vertical lines are average error bars retrieved from  
 337 the harmonic analysis. The seasonal trends for all the tides are the same at 90 m and 300 m  
 338 depths.

339 A fortnightly oscillation is present only in the summers at all depths, as seen in Table S2, as well  
 340 as in the raw pressure data (Fig. 5). At the same time, it is not found significant in the spectral  
 341 analysis shown in Fig. 6. This might be explained by non-linear interactions between semidiurnal  
 342 and diurnal tides which have been argued to amplify the oscillations (Kwong et al., 1997). In Fig.

343 5, a reconstruction of only the M2 and S2 tides shows the spring and neap tides, similar to the  
344 fortnightly oscillations observed in the raw data emphasized in the bottom graph.

345

346 Another significant tide identified was the UPS1 tide (Table S2). The amplitude range is wide  
347 from 0.5-10 cm at 90 m with no apparent pattern regarding changes between seasons apart from  
348 winter months, where the largest amplitudes were found. The UPS1 oscillation is less  
349 considerable in the pressure analysis than in the currents detailed in section 3.2.1. The UPS1 tide  
350 has been observed in sea level variability analysis in Alexandria (El-Geziry & Radwan, 2012; El-  
351 Geziry 2021; Khedr et al., 2018) with amplitudes below 1.5 cm. These results were taken from  
352 tide gauges along the Port of Alexandria. However, the UPS1 tide found can possibly be  
353 attributed to near-inertial internal waves due to the clockwise motion of the current  
354 measurements when the UPS1 tide is present (not shown). Motions in the near-inertial regime  
355 can generate near-internal waves that do not only oscillate in a purely horizontal plane, such as  
356 inertial oscillations, but also vertically, albeit with much smaller vertical amplitudes than internal  
357 tides (Alford et al., 2016). The amplitude of this tidal constituent declines with depth over all  
358 seasons, which is also consistent with near-inertial oscillations.

359

360 Tidal constituents represent a significant portion of the variance of the pressure time series for  
361 most of the year. The variance variation in 2017 regarding season and depth is demonstrated in  
362 Table 2. Before analyzing the trends in the table, it is important to note a few anomalies of 2017  
363 from the other years used in this research. The variance in the spring is unusually high, with the  
364 variance in 2018 and 2020 at  $1.1 \cdot 10^{-2}$  for all depths apart from 1300, for which we do not have  
365 further data. Furthermore, summer and fall percentages are uncharacteristically small, with  
366 summer percentages starting around 40% and fall percentages around 70%. With that, the  
367 general trends found in Table 2 are relevant and similar for all the years in the study.

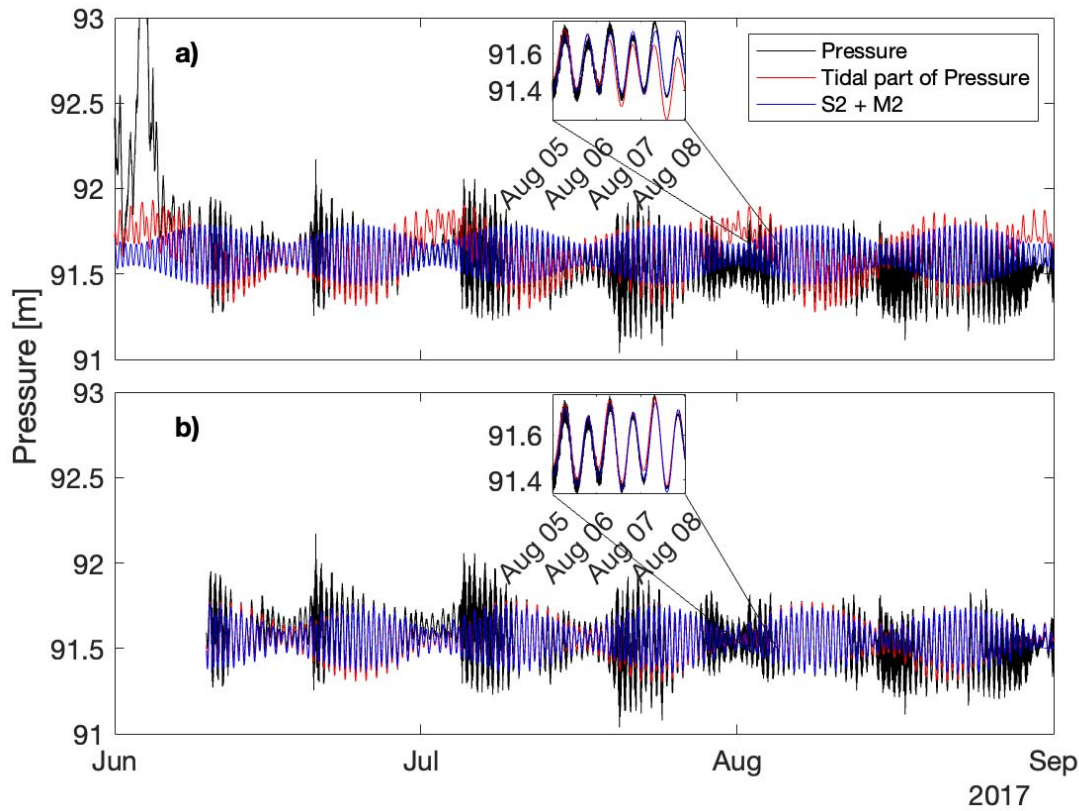
368

369 With depth, for all the seasons except fall, we see a slight drop in tidal variance for the top 300  
370 meters and a decline to what appears to be a baseline variance of approximately  $1.1 \cdot 10^{-2}$  m at  
371 1300 m. The opposite can be said for the role of the tides in the total variance, which increases  
372 with depth due to the waning effects of atmospheric forces with depth. At 1300 m, seasonal  
373 changes of tidal variance are negligible, while for the percentages, we see that seasonal changes  
374 continue to appear in the deep. With seasonality, at the top 300 m, the variance and percentages  
375 vary from the baseline variance in winter and summer in all the years of the dataset, except  
376 spring 2017. Winter is found to have the greatest variance, then summer with a smaller variance.  
377 Fall is the season with the highest percentage of tidal variance from the total variance, then  
378 summer and spring with roughly similar numbers, and winter with the least tidal variance from  
379 the total variance.

380

	Winter	Spring	Summer	Fall
90m	$2.5 \cdot 10^{-2}$ ( <b>2.7%</b> )	$4.7 \cdot 10^{-2}$ ( <b>19.9%</b> )	$1.8 \cdot 10^{-2}$ ( <b>24.2%</b> )	$1.1 \cdot 10^{-2}$ ( <b>49.3%</b> )
200m	-	-	$1.8 \cdot 10^{-2}$ ( <b>25.1%</b> )	$1.1 \cdot 10^{-2}$ ( <b>52.2%</b> )
300m	$2.2 \cdot 10^{-2}$ ( <b>2.9%</b> )	$4.2 \cdot 10^{-2}$ ( <b>20.4%</b> )	$1.7 \cdot 10^{-2}$ ( <b>25.8%</b> )	$1.1 \cdot 10^{-2}$ ( <b>54.1%</b> )
1300m	$1.1 \cdot 10^{-2}$ ( <b>20.6%</b> )	$1.1 \cdot 10^{-2}$ ( <b>41.4%</b> )	$1 \cdot 10^{-2}$ ( <b>77.2%</b> )	$1.1 \cdot 10^{-2}$ ( <b>84%</b> )

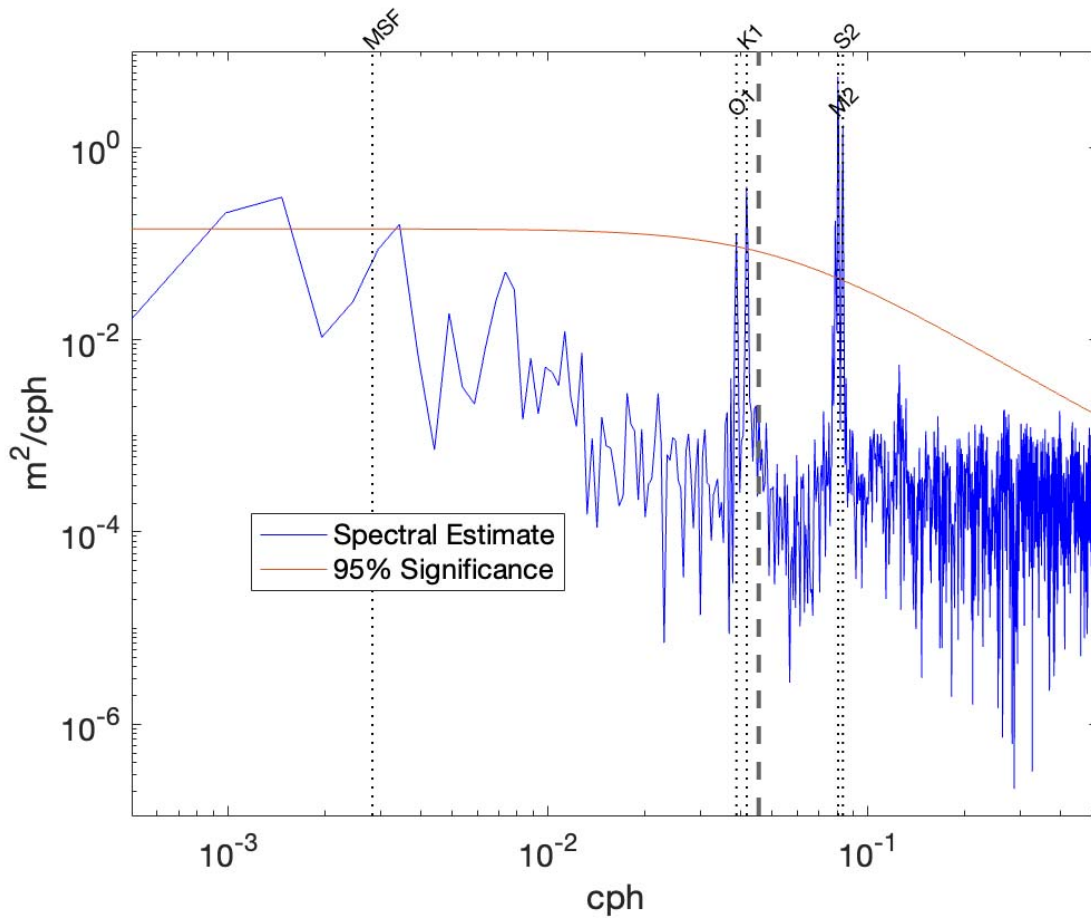
381 **Table 2.** Total tidal variance in m and the percentage of the tidal variance (in bold) from the total  
 382 variance of the pressure time series found per season of 2017 and at four depths. Only tidal  
 383 constituents with an SNR of above one are considered in the tidal variance.



384

385 **Figure 5.** A sample of the pressure time series in m at 90 m from summer 2017 where the top  
 386 graph includes a sudden pressure jump in the analysis and the bottom graph the pressure jump is  
 387 excluded from the analysis. Both graphs include the raw time series (black), the reconstruction of  
 388 the amplitudes of all the significant tides of the season (red), and the reconstruction of only the  
 389 S2 and M2 (blue). In the inset, there is a zoom-in on a three-day interval in August. It is clear  
 390 from both graphs the importance of the significant tides, and specifically the semidiurnal tides,  
 391 on the pressure. From the zoom-in of both graphs, we can see that the pressure jump distorts the

392 harmonic analysis, where the total reconstruction (red) behaves differently between the two  
 393 graphs.



394

395 **Figure 6.** The Power Spectral Density in  $\text{m}^2/\text{cph}$  of the pressure time series as a function of cph  
 396 (log-log) at 300 m depth in the summer of 2017. The dashed vertical lines in the graph indicate  
 397 tide constituents; Msf, O1, K1, M2, and S2. The red curve indicates the 95% Significance Level  
 398 with respect to red noise. The diurnal and semidiurnal amplitudes are significant in the spectrum.  
 399 The MSF fortnightly oscillation peak is seen to be insignificant in the spectral analysis as  
 400 opposed to the tidal harmonic analysis.

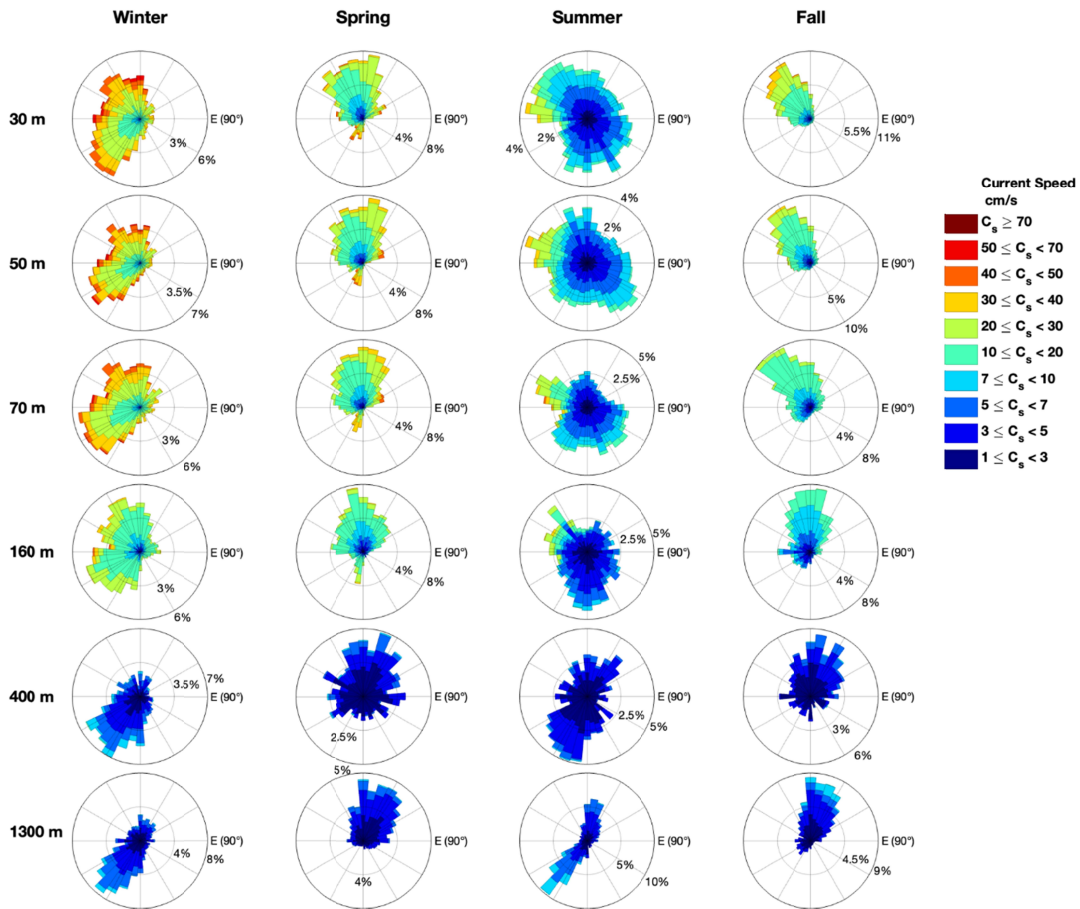
401

### 402 3.2 Current Variability

403

404 The currents were dominated by episodes of strong flows, particularly in the winter, as seen in  
 405 Table 3 and Fig. 7 and 8.

406



407

408 **Figure 7.** Current rose of the currents at the depths of 30 m, 50 m, 70 m, 160 m, 400 m, and  
 409 1300 m during the winter, spring, summer, and fall periods of 2017. The units of the current rose  
 410 are in cm/s. Each record of a given current in a times series is projected in its direction and added  
 411 to a bin matching the ranges in the legend. The larger the bin size, the more frequently the speed  
 412 counted in that direction. The approximate frequencies of occurrence can be seen by the  
 413 percentages shown.

414

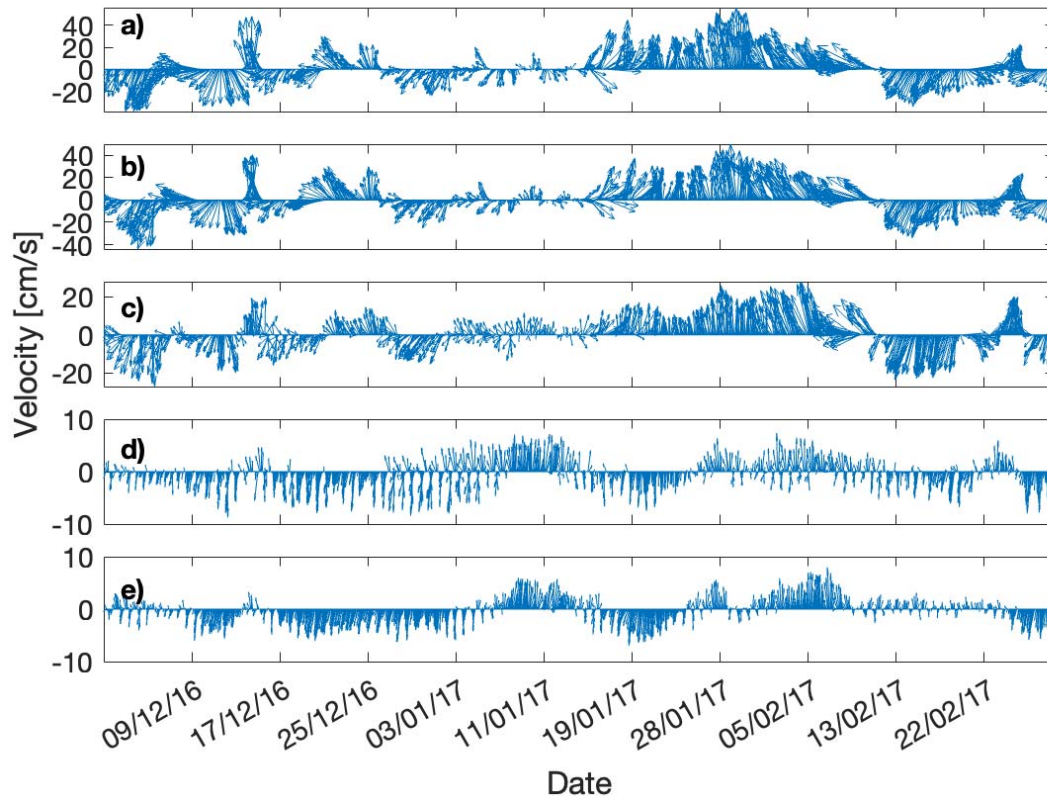
415

	<b>Maximum recorded speed</b>	<b>Date of max recorded speed</b>	<b>Winter mean speed</b>	<b>Spring mean speed</b>	<b>Summer mean speed</b>	<b>Fall mean speed</b>
<b>30m</b>	78.4	30-Dec-18 15:45:00	20.5	14.1	9	12.6
<b>50m</b>	74.4	30-Dec-18 05:15:00	20.4	14.1	9	10.7
<b>70m</b>	68.8	10-Jan-19 16:30:00	19.2	13.8	8.7	8.7
<b>160m</b>	43.2	10-Feb-17 19:00:00	11.3	9.2	5.8	5.4
<b>400m</b>	19.9	13-Jan-19 00:00:00	4	3	2.7	2.4
<b>1300m</b>	12.2	06-Jan-18 12:00:00	2.3	2	1.2	1

416 **Table 3.** Maximum recorded speeds (magnitude of the horizontal currents) at different depths  
417 (cm/s) were found in all the years of the dataset (cm/s) and the dates they were found. Season  
418 mean results are the season average from the three years of observations.

419

420 In Table 3, a weakening in speed with depth is evident, and a smaller dependency of the seasons  
421 on the speed at 1300 m. The flow across the entire water column is mainly meridional (roughly  
422 parallel to isobath); an example is shown in the feather diagram in Fig. 8.



423

424 **Figure 8.** A feather diagram showing the currents (cm/s) during winter 2017. Each subplot  
 425 depicts a different depth, in ascending order of 30 m, 70 m, 160 m, 400 m, and 1300 m. The  
 426 velocities of 30 m, 70 m, 160 m, and 1300 m depths were averaged for a two-hour sampling  
 427 period. Note the different scales for the different depths.

428

429 A dominant flow direction at the near-surface is toward the north in the spring. At the same time,  
 430 an almost sporadic motion occurs in the summer (Fig. 7). The continental shelf break is parallel  
 431 to the coast (Fig. 1), and in the fall, the near-surface currents move perpendicularly away from  
 432 the shelf. The winter also shows movement away from the shelf but no specific direction. At  
 433 1300 m depth, the directions of currents are split between northwest, along the shelf break,  
 434 during spring and fall, and southeast during the summer and winter.

435

### 436 3.2.1 Tidal Harmonic Analysis of Current Variability

437

438 For the four main tidal constituents of the study, O1, K1, M2, and S2, different results arise from  
 439 the current analysis than from the pressure analysis. The UPS1 is the single most prominent tide  
 440 in the tidal harmonic analysis done on the currents, yet it can be attributed to the near-inertial  
 441 band and will not be discussed further in the results.

442

443 The S2 and M2 are significant sporadically near the surface, with nearly negligible magnitudes  
444 of roughly 0.3 cm/s for the S2 and between 0.3-0.6 cm/s for the M2, as seen in Table S3. For the  
445 M2, this is an order of magnitude weaker than the drifter data found in Poulain et al. (2018).  
446 Still, for the S2, the results are consistent with Poulain et al. (2018) findings, which show  
447 currents between 0-1 cm/s, while the results from the drifter data are generally larger for both the  
448 15-day (0.6-3 cm/s) and 30-day (0.7-1.3 cm/s) analysis. The OSU TPXO model finds a semi-  
449 major ellipse axis for the M2 current of 9.7 cm/s and 5.8 cm/s for the S2 tidal current, with  
450 values larger than those in this study. At 1300 m, the S2 and M2 are significant across the  
451 seasons, with magnitudes of 0.1-0.2 cm/s for M2 and 0.1-0.2 cm/s for the S2 tide (Table S3).

452

453 An opposite trend occurs for the diurnal tides. At 30 m, the K1 (Table S3) tidal constituent is  
454 significant across all seasons, ranging from 0.9-3 cm/s. Seasonal variability is present, with fall  
455 being the strongest season and summer-spring the weakest tidal currents. With depth, K1 starts to  
456 be less significant until 1300 m, where the constituent is not significant across all seasons. This  
457 might be due to intense wind stress originating from the daily breeze, as suggested by Alvarez et  
458 al. (2003), Poulain et al. (2018), and others. The O1 tidal currents are also less significant with  
459 depth, as seen in Table S3, with a range of velocities between 0.9-1.9 cm/s at all depths. In most  
460 segments, the analysis did not find significant oscillations of the O1 tide.

461

462 The variance of the significant tidal constituents plays a minor part in the overall current  
463 variance, depicted in Table 4. Feliks et al. (2022) showed that the intraseasonal oscillations are  
464 generally larger (above 4 cm/s) than the tides in the Eastern Mediterranean shown here. The  
465 results which are inconsistent with the other years are the weak top 160 m in the winter, which  
466 are typically above 10 cm/s and have a much higher percentage of variance, and the large  
467 variance found in the fall at 70 m with a smaller than usual percentage for the top 50 m in the  
468 same season. At 1300 m in fall, there is a very low tidal variance, yet we can not with confidence  
469 that this is out of the ordinary since we do not have any more data about the fall season of a  
470 different year.

471

472 The general trends in 2017, shown in Table 4 and the rest of the analyzed data, show stronger  
473 tidal currents in the winter and spring, with a slump in summer. As in the pressure analysis, tidal  
474 variance lessens with depth, yet the percentage of tidal variance from total variance grows with  
475 depth. Unlike with the pressure analysis, it doesn't seem like there is a baseline variance.

476

	Winter	Spring	Summer	Fall
<b>30m</b>	-	35.9 (16.5%)	5.4 (18.4%)	6.9 (4.7%)
<b>50m</b>	3.4 (0.6%)	37.3 (17%)	8.2 (13.2%)	4.4 (4.7%)
<b>70m</b>	3.2 (0.6%)	34.7 (16.7%)	8.2 (13.5%)	19.43 (30.4%)
<b>160m</b>	2.8 (1.2%)	13.7 (14.2%)	4.2 (11%)	5.9 (17%)
<b>400m</b>	2.8 (18.3%)	1.5 (21.8%)	2 (35.2%)	2.5 (36.7%)
<b>1300m</b>	2.8 (22.1%)	1.6 (20.9%)	1.6 (10.1%)	0.1 (1.2%)

477 **Table 4.** Total tidal variance in cm/s and the percentage of the tidal variance (in bold) from the  
478 total variance of the current time series found per season of 2017 and at four depths. Total tidal  
479 variance is taken from the T\_Tide package as the summation of the total tidal variance of u and  
480 v. Only tidal constituents with an SNR above 1 are considered in the tidal variance.

481

### 482 3.2.2 Sensitivity to Dataset Lengths

483

484 The data of four seasons from 2017 from DeepLev is analyzed using tidal harmonic analysis in  
485 different dataset lengths of 15-day, 22-day, and 30-day, at three different depths of 70 m, 160 m,  
486 and 1300 m.

487

488 At 70 m depth, on average across all seasons, the M2 tide magnitude from a 15-day analysis is  
489 approximately 1.3 times larger than the 22-day analysis and 1.6 times larger than the 30-day  
490 analysis. For the S2 tide magnitude, a 15-day analysis is approximately 1.1 times larger than a  
491 22-day analysis and 1.4 times larger than a 30-day analysis. The 22-day period is larger than the  
492 30-day, for the M2 magnitude, by only 1.2; for the S2, it is 1.4 times larger.

493

494 At 160 m depth, on average across all seasons, the M2 tide magnitude from a 15-day analysis is  
495 approximately 1.3 times larger than the 22-day analysis and 1.9 times larger than the 30-day  
496 analysis. For the S2 tide magnitude, a 15-day analysis is approximately 1.5 times larger than a  
497 22-day analysis and 1.8 times larger than a 30-day analysis. The 22-day period is larger than the  
498 30-day, for the M2 magnitude, by 1.4; for the S2, it is 1.5 times larger.

499

500 At 1300 m depth, on average across all seasons, the M2 tide magnitude from a 15-day analysis is  
501 approximately 1.2 times larger than the 22-day analysis and 1.1 times larger than the 30-day  
502 analysis. For the S2 tide magnitude, a 15-day analysis is 0.9 times larger than the 22-day analysis  
503 (this may be due to a lack of significant tides across the seasons, as shown in Table S4) and 1.3  
504 times larger than the 30-day analysis. The 22-day period is the same as the 30-day for the M2  
505 magnitude, while for the S2, it is 1.4 times larger.

506

507 These results are consistent with the leakage effects of two close frequencies analyzed at exactly  
508 their Rayleigh criterion and not their “well-resolved” criterion. In summary, the 15-day analysis  
509 for the M2 and S2 results is larger in magnitude than the 22-day analysis, which is larger than the  
510 30-day analysis. Appendix D-1 contains a table with the results from the tidal harmonic analysis  
511 of the mooring results.

512

### 513 **3.3 Tidal Harmonic Analysis Based on Drifter Data vs. Moored Instruments**

514

515 Drifter data has been used to estimate harmonic tidal constituents, both globally (Poulain 2015)  
516 and regionally (Poulain 2018; Lie et al., 2002; Ohshima et al., 2002) or to compare with tidal  
517 prediction models (Zaron & Elipot 2021; Kodaira 2016; Zaron & Ray 2017; Crawford et al.,  
518 1998;). Using drifters for tidal current analysis has the benefit of inexpensive observations with  
519 short sampling intervals at a distance from the coast, where most of the moored devices are  
520 stationed. Lie et al. (2002) demonstrated this in the Yellow Sea.

521

522 In the following tidal analysis, we tested the sensitivity of the semidiurnal tidal constituent  
523 results from a tidal analysis done on drifters using different dataset lengths. The results were also  
524 compared with current data from DeepLev. The Rayleigh criterion for the S2 and M2  
525 constituents is approximately 15 days, yet the stricter “well-defined” criterion is approximately  
526 22 days. We used 15, 22, and 30-day datasets for our comparative analysis. We only took drifter  
527 trajectories within 1° of DeepLev to limit the spatial variations in tidal regimes.

528

#### 529 **3.3.1 Tidal Harmonic Analysis of Drifter Data from 15-Day Segments**

530

531 Complete details of the drifter data following a tidal harmonic analysis can be found in Appendix  
532 D-2. For many segments fitting the predefined criteria, the dominant tide was the S2 tide, as seen

533 in Table 5. Interestingly, the S2 results show a decrease in the magnitude of the tide with the  
 534 coming of summer, agreeing with the results shown in section 3.2.

535

536 As a comparison with the drifters, a tidal harmonic analysis was done on data from DeepLev  
 537 from the same dates at 50 m depth, which did not show an explicit dominant tidal constituent and  
 538 generally smaller magnitudes. It is clear from the moored dataset that the semidiurnal tides are  
 539 almost the same, yet the magnitudes reported in DeepLev are much smaller for the S2 tide while  
 540 only slightly smaller for the M2. The magnitudes are also larger than those found in section  
 541 3.2.1, which agrees with signal analysis theory.

542

543 These results agree with the results found by Poulain et al. (2018), which find both the S2 and  
 544 M2 with a magnitude of under 2 cm/s. A few notes are important to emphasize. First, the  
 545 averages were calculated without regard to results with an SNR of below 1. Second, the summer  
 546 results include segments from the summer of 2017 and 2018. Lastly, the S2 and M2 magnitude  
 547 behavior, i.e., S2 being greater than M2, was found in different drifter types and years.

548

	<b>M2 - Drifters</b>	<b>M2 - Mooring</b>	<b>S2 - Drifters</b>	<b>S2 - Mooring</b>
<b>Winter</b>	1.7	0.9	1.9	0.9
<b>Spring</b>	1.6	0.9	0.7	0.9
<b>Summer</b>	1.5	0.8	0.8	0.7
<b>Fall</b>	2	0.6	1	0.5

549

550 **Table 5.** Seasonal average magnitudes [cm/s] of the M2 and S2 tidal currents from drifters and  
 551 DeepLev in 15-day segments.

552

### 553 **3.3.2 Tidal Harmonic Analysis of Drifter Data from 22-Day Segments**

554

555 The results, as seen in Table 6 from the drifters' 22-day segments, were, in general, smaller in  
 556 magnitude than the results from the 15-day segments, a result that is consistent with theory and  
 557 seen in section 3.2.2. The dominant S2 seen in the 15-day drifters also subsided and is almost the  
 558 same as the M2 apart for the summer and fall results, with fall containing only one segment. As  
 559 for the results from DeepLev, the magnitudes were roughly the same for both the 15 and 22-day  
 560 segments. It is important to note that by raising the time limit to 22 days, fewer segments were  
 561 used, with fewer significant results for the tides. Complete details of the relevant drifter segments  
 562 following a tidal harmonic analysis can be found in Appendix D-3.

563

	<b>M2 - Drifters</b>	<b>M2 - Mooring</b>	<b>S2 - Drifters</b>	<b>S2 - Mooring</b>
<b>Winter</b>	1.1	1	1.2	N/S
<b>Spring</b>	1.4	0.8	1.1	0.6
<b>Summer</b>	0.8	0.8	1.3	0.5
<b>Fall</b>	N/S	N/S	2	N/S

564

565 **Table 6.** Seasonal average magnitudes [cm/s] of the M2 and S2 tidal currents from drifters and  
 566 DeepLev in 22-day segments. N/S indicates values with a signal-to-noise ratio below 1 in the  
 567 tidal analysis.

568

### 569 3.3.3 Tidal Harmonic Analysis of Drifter Data from 30-Day Segments

570

571 Only seven drifter segments were found to be 30 days near DeepLev. Full details of the drifter  
 572 data following a tidal harmonic analysis can be found in Appendix D-4. Unfortunately, there is a  
 573 gap in the mooring data around when the drifters were in its proximity, so few results can be  
 574 compared. An example of a drifter's 30-day trajectory can be found in Fig. 9 with what seems  
 575 like near-inertial oscillations of the drifter.

576

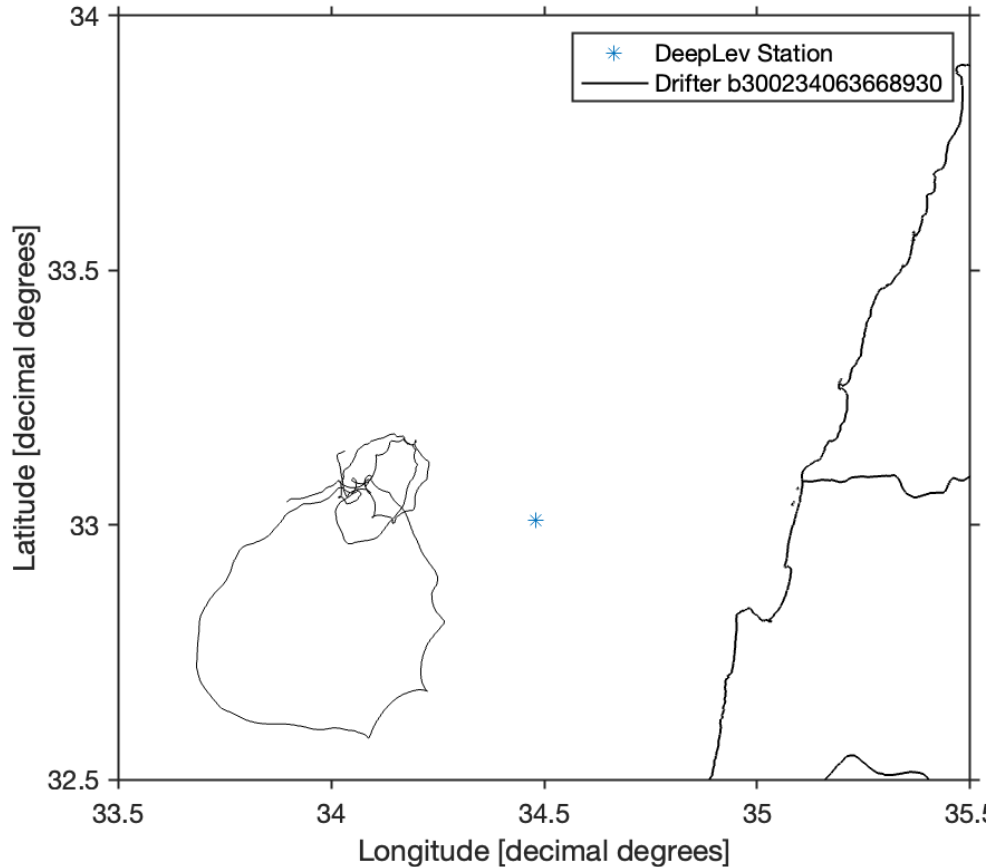
	<b>M2 - Drifters</b>	<b>M2 - Mooring</b>	<b>S2 - Drifters</b>	<b>S2 - Mooring</b>
<b>Winter</b>	N/D	N/D	N/D	N/S
<b>Spring</b>	N/S	0.7	1.2	0.6
<b>Summer</b>	0.8	0.6	0.6	0.5
<b>Fall</b>	N/D	N/D	N/D	N/S

577

578 **Table 7.** Seasonal average magnitudes [cm/s] of the M2 and S2 tidal currents from drifters and  
579 DeepLev in 22-day segments. N/S indicates values with a signal-to-noise ratio below 1 in the  
580 tidal analysis. N/D indicates areas with no data.

581

582 To summarize the tidal harmonic analysis on different drifter dataset lengths, the results show a  
583 weakening of magnitude of the M2 and S2 tide as the dataset grew longer. This was less  
584 pronounced in the equivalent mooring dataset, yet the trend remained.



585

586 **Figure 9.** Example of the trajectory of drifter b300234063668930, surrounding DeepLev  
 587 (marked by a blue star), used to analyze the semidiurnal tidal constituents M2 and S2 between  
 588 27-Apr-2017 06:00:00 and 27-May-2017 05:00:00.

589

#### 590 **4. Discussion & Conclusions**

591

592 Data from both the moored mooring station and surface drifters in its vicinity were used to study  
 593 the structure of tides both from currents and pressure in the Eastern Levantine basin at  
 594 semidiurnal (M2 and S2), diurnal (K1 and O1) and longer (Msf) periods. The pressure variance  
 595 explained by the tides is substantial at all seasons apart from the winter, with the most significant  
 596 season being the fall (average of 67% explained variance), increasing in explained variance with  
 597 depth. Unlike the pressure, the variance of the current explained by the tides is less considerable,  
 598 with little variation with depth and spring holding the highest portion of tidal explained variance  
 599 (average of 19%). A much larger variance is explained by intraseasonal variability (Feliks et al.,  
 600 2022).

601

602 The M2 was the most dominant frequency with amplitudes similar to both tide gauge and model  
603 results (Tsimplis et al., 1995; Arabelos et al., 2011). No variability due to seasonal changes was  
604 evident in the M2 amplitude. For the S2, a change in amplitude of 2 cm can be discerned  
605 between summer and fall averages. Even with this variability, previous studies and the OSU  
606 TPXO model show that this range generally agrees with previous results. As proposed  
607 previously, the seasonal variation of tides can result from several reasons. Müller et al. (2014)  
608 argued that stronger stratification leads to less loss of energy from the barotropic tide to  
609 turbulence and mixing, and Ray (2022) proposed that compound tides with frequencies very near  
610 the vicinity of the M2 tide as well as astronomical modulations of the Sun's third-body  
611 perturbations of the lunar orbit play a role in the observed seasonality of the M2 tide alongside  
612 climate processes.

613

614 Sharp variability due to the change of seasons and depths was found in the K1 signal, with  
615 amplitudes reaching up to 10 cm in the winter at depths near the surface, significantly higher  
616 than previously reported, and down to 2-3 cm in the summer, slightly larger than the models and  
617 observations. Although out of the scope of this paper, rudimentary seasonal spectral analysis of  
618 coastal wind speed from a meteorological site on the Israeli coast shows strong semidiurnal and  
619 diurnal frequencies during the winter as opposed to the rest of the year. Another possible  
620 explanation for these results is mooring motions unrelated to the tides.

621

622 The weak semidiurnal tidal currents from the mooring device are qualitatively consistent with  
623 the literature (Pugh, 1987; Poulain et al., 2018) with ranges below 1 cm/s. Diurnal tides,  
624 especially the K1, are all above 1 cm/s near the surface, with fall currents averaging 2.2 cm/s.  
625 These might be attributed to the diurnal breeze, as alluded to before.

626

627 The most dominant tidal current found was the UPS1, with values reaching up to 5 cm/s. It is  
628 significant in all seasons and depths. This result possibly comes from the leakage of the near-  
629 inertial band and sensitivity to data set length. When taking larger datasets than the seasonal 90-  
630 day used here, such as 120-day and 180-day (not shown), we found this dominant frequency  
631 shifts away from the UPS1 tide and closer to 21.99 h, the inertial frequency at DeepLev. It is also  
632 evident that the signal found in rotary spectra done on the current time series shows the  
633 frequency as a predominantly clockwise motion (not shown).

634

635 DeepLev allowed the assessment of the criteria needed of surface drifters, in terms of temporal  
636 resolution, to give an adequate picture of a local tidal regime. The widely accepted Rayleigh  
637 criterion (further details in Thomson & Emery, 2014) of  $\Delta f = \frac{1}{T}$  gives "just resolved" peaks,  
638 which, we argue in this paper, are contaminated due to leakage. The detailed findings in sections  
639 3.2.2 and 3.3.1 illustrate this leakage in this local scenario. "Well resolved" peaks can be  
640 achieved with a constraint of  $\Delta f > \frac{3}{2T}$ . Although we have shown large amplitude changes when

641 analyzing different dataset lengths, only a few relevant drifters were available near DeepLev, a  
642 serious impediment when adopting a stricter temporal constraint. All the results found by the  
643 surface drifters, regardless of dataset length, were larger ( $>1$  cm/s) than the results found in  
644 moored datasets ( $<1$  cm/s).

645

## 646 **Acknowledgments**

647 This study was supported by the Israeli Ministry of Science and the Italian Ministry of Foreign  
648 Affairs.

## 649 **Open Research**

650 Data from the DeepLev Mooring site were used to create this manuscript, and all the code and  
651 datasets needed to recreate the figures and results in this manuscript can be found at  
652 [10.5281/zenodo.7979160](https://doi.org/10.5281/zenodo.7979160). The OSU TPXO Barotropic Tide Model was used, considering the  
653 DeepLev mooring location (Lat= 33N03.67, Lon=34E29.296). The TPXO model was retrieved  
654 using the TMD v 2.5 for Matlab (S. Erofeeva, L. Padman, and S. L. Howard (2020). Tide Model  
655 Driver (TMD) version 2.5, Toolbox for Matlab  
656 ([https://www.github.com/EarthAndSpaceResearch/TMD\\_Matlab\\_Toolbox\\_v2.5](https://www.github.com/EarthAndSpaceResearch/TMD_Matlab_Toolbox_v2.5)), GitHub.  
657 Retrieved [28.5.2023].). The current rose figure was made with Windrose version 200305  
658 (Daniel Pereira (2023). Wind Rose  
659 (<https://www.mathworks.com/matlabcentral/fileexchange/47248-wind-rose>), MATLAB Central  
660 File Exchange. Retrieved May 28, 2023.). Tidal analysis was done using the T\_Tide toolbox (R.  
661 Pawlowicz, B. Beardsley, and S. Lentz, "Classical tidal harmonic analysis including error  
662 estimates in MATLAB using T\_TIDE", *Computers and Geosciences* 28 (2002), 929-937)  
663 version 1.3b downloaded from [https://www.eoas.ubc.ca/~rich/t\\_tide/t\\_tide\\_v1.3beta.zip](https://www.eoas.ubc.ca/~rich/t_tide/t_tide_v1.3beta.zip). PSD  
664 figures were produced and analyzed using the JLAB toolbox (Lilly, J. M. (2021), jLab: A data  
665 analysis package for Matlab, v. 1.7.0, <http://www.jmlilly.net/software>).

666 Bathymetric Map of Eastern Mediterranean was created using M\_Map (Pawlowicz, R., 2020.  
667 "M\_Map: A mapping package for MATLAB", version 1.4m, [Computer software], available  
668 online at [www.eoas.ubc.ca/~rich/map.html](http://www.eoas.ubc.ca/~rich/map.html)).

669

## 670 **References**

671 Albérola, C., Rousseau, S., Millot, C., Astraldi, M., Font, J., García-Lafuente, J., ... &  
672 Vangriesheim, A. (1995). Tidal currents in the western Mediterranean Sea. *Oceanologica Acta*,  
673 *18*(2), pp.273-284. <http://hdl.handle.net/10261/194257>

674

675 Alford, M. H., MacKinnon, J. A., Simmons, H. L., & Nash, J. D. (2016). Near-inertial internal  
676 gravity waves in the ocean. *Annual review of marine science*, *8*, 95-123.

677 <http://dx.doi.org/10.1146/annurev-marine-010814-015746>

678

679 Álvarez, O., Tejedor, B., Tejedor, L., & Kagan, B. A. (2003). A note on sea-breeze-induced  
680 seasonal variability in the K1 tidal constants in Cádiz Bay, Spain. *Estuarine, Coastal and Shelf*  
681 *Science*, *58*(4), 805-812. [https://doi.org/10.1016/S0272-7714\(03\)00186-0](https://doi.org/10.1016/S0272-7714(03)00186-0)

682

683 Arabelos, D. N., Papazachariou, D. Z., Contadakis, M. E., & Spatalas, S. D. (2011). A new tide  
684 model for the Mediterranean Sea based on altimetry and tide gauge assimilation. *Ocean*

685 *Science*, *7*(3), 429-444. <https://doi.org/10.5194/os-7-429-2011>

686

687 Bendat, J. S., & Piersol, A. G. (2011). *Random data: analysis and measurement procedures*.

688 Hoboken, NJ: John Wiley & Sons.

689

690 Carrère, L., Le Provost, C., & Lyard, F. (2004). On the statistical stability of the M2 barotropic  
691 and baroclinic tidal characteristics from along-track TOPEX/Poseidon satellite altimetry  
692 analysis. *Journal of Geophysical Research: Oceans*, 109(C3).

693 <https://doi.org/10.1029/2003JC001873>

694

695 Chavanne, C., Janeković, I., Flament, P., Poulain, P. M., Kuzmić, M., & Gurgel, K. W. (2007).  
696 Tidal currents in the northwestern Adriatic: High-frequency radio observations and numerical  
697 model predictions. *Journal of Geophysical Research: Oceans*, 112(C3).

698 <https://doi.org/10.1029/2006JC003523>

699

700 Cosoli, S., Drago, A., Ciruolo, G., & Capodici, F. (2015). Tidal currents in the Malta–Sicily  
701 Channel from high-frequency radar observations. *Continental Shelf Research*, 109, 10-23.

702 <https://doi.org/10.1016/j.csr.2015.08.030>

703

704 Deparis, V., Legros, H., & Souchay, J. (2013). Investigations of Tides from the Antiquity to  
705 Laplace. *Tides in astronomy and astrophysics*, 31-82. [https://doi.org/10.1007/978-3-642-32961-](https://doi.org/10.1007/978-3-642-32961-6_2)

706 [6\\_2](https://doi.org/10.1007/978-3-642-32961-6_2)

707

708 Egbert, G. D., & Erofeeva, S. Y. (2002). Efficient inverse modeling of barotropic ocean tides.  
709 *Journal of Atmospheric and Oceanic Technology*, 19(2), 183-204. [https://doi.org/10.1175/1520-](https://doi.org/10.1175/1520-0426(2002)019<0183:EIMOBO>2.0.CO;2)

710 [0426\(2002\)019<0183:EIMOBO>2.0.CO;2](https://doi.org/10.1175/1520-0426(2002)019<0183:EIMOBO>2.0.CO;2)

711

712 El-Geziry, T., & Radwan, A. (2012). Sea level analysis off Alexandria, Egypt. *The Egyptian*  
713 *Journal of Aquatic Research*, 38(1), 1-5. <https://doi.org/10.1016/j.ejar.2012.08.004>

714

715 El-Geziry, T. M. (2021). Sea-level, tides and residuals in Alexandria Eastern Harbour,  
716 Egypt. *The Egyptian Journal of Aquatic Research*, 47(1), 29-35.

717 <https://doi.org/10.1016/j.ejar.2020.10.003>

718

719 Ferrarin, C., Bellafiore, D., Sannino, G., Bajo, M., & Umgiesser, G. (2018). Tidal dynamics in  
720 the inter-connected Mediterranean, Marmara, Black and Azov seas. *Progress in*

721 *Oceanography*, 161, 102-115. <https://doi.org/10.1016/j.pocean.2018.02.006>

722

723 Feliks, Y., & Itzikowitz, S. (1987). Movement and geographical distribution of anticyclonic  
724 eddies in the Eastern Levantine Basin. *Deep Sea Research Part A. Oceanographic Research*  
725 *Papers*, 34(9), 1499-1508. [https://doi.org/10.1016/0198-0149\(87\)90105-1](https://doi.org/10.1016/0198-0149(87)90105-1)

726

727 Feliks, Y., Gildor, H., & Mantel, N. (2022). Intraseasonal oscillatory modes in the Eastern  
728 Mediterranean Sea. *Journal of Physical Oceanography*. <https://doi.org/10.1175/JPO-D-21->

729 [0185.1](https://doi.org/10.1175/JPO-D-21-0185.1)

730

731 Garcia-Gorriz, E., Candela, J., & Font, J. (2003). Near-inertial and tidal currents detected with a  
732 vessel-mounted acoustic Doppler current profiler in the western Mediterranean Sea. *Journal of*

733 *Geophysical Research: Oceans*, 108(C5). <https://doi.org/10.1029/2001JC001239>

734

- 735 Gasparini, G. P., Smeed, D. A., Alderson, S., Sparnocchia, S., Vetrano, A., & Mazzola, S.  
736 (2004). Tidal and subtidal currents in the Strait of Sicily. *Journal of Geophysical Research:*  
737 *Oceans*, 109(C2). <https://doi.org/10.1029/2003JC002011>  
738
- 739 Hansen, D. V., & Poulain, P. M. (1996). Processing of WOCE/TOGA drifter data. *Journal of*  
740 *Atmospheric and Oceanic Technology*, 13(4), 900-909. [https://doi.org/10.1175/1520-](https://doi.org/10.1175/1520-0426(1996)013<0900:QCAIOW>2.0.CO;2)  
741 [0426\(1996\)013<0900:QCAIOW>2.0.CO;2](https://doi.org/10.1175/1520-0426(1996)013<0900:QCAIOW>2.0.CO;2)  
742
- 743 Hsieh, H. L., Fan, L. F., Chen, C. P., Wu, J. T., & Liu, W. C. (2010). Effects of semidiurnal tidal  
744 circulation on the distribution of holo-and meroplankton in a subtropical estuary. *Journal of*  
745 *Plankton Research*, 32(6), 829-841. <https://doi.org/10.1093/plankt/fbq026>  
746
- 747 Kar, S., Ghosh, I., Chowdhury, P., Ghosh, A., Aitch, P., Bhandari, G., & RoyChowdhury, A.  
748 (2022). A model-based prediction and analysis of seasonal and tidal influence on pollutants  
749 distribution from city outfalls of river Ganges in West Bengal, India and its mapping using GIS  
750 tool. *PLOS Water*, 1(2), e0000008. <https://doi.org/10.1371/journal.pwat.0000008>  
751
- 752 Katz, T., Weinstein, Y., Alkalay, R., Biton, E., Toledo, Y., Lazar, A., ... & Herut, B. (2020). The  
753 first deep-sea mooring station in the eastern Levantine basin (DeepLev), outline and insights into  
754 regional sedimentological processes. *Deep Sea Research Part II: Topical Studies in*  
755 *Oceanography*, 171, 104663. <https://doi.org/10.1016/j.dsr2.2019.104663>  
756

- 757 Khedr, A. M., Abdelrahman, S. M., & El-Din, K. A. A. (2018). Currents and sea level variability  
758 of Alexandria coast in association with wind forcing. *Journal of King Abdulaziz*  
759 *University*, 28(2), 27-42. <http://dx.doi.org/10.4197/Mar.28-2.3>  
760
- 761 Kwong, S. C., Davies, A. M., & Flather, R. A. (1997). A three-dimensional model of the  
762 principal tides on the European shelf. *Progress in Oceanography*, 39(3), 205–262.  
763 [https://doi.org/10.1016/S0079-6611\(97\)00014-1](https://doi.org/10.1016/S0079-6611(97)00014-1)  
764
- 765 Kunze, E. (1985). Near-inertial wave propagation in geostrophic shear. *Journal of Physical*  
766 *Oceanography*, 15(5), 544–565. [https://doi.org/10.1175/1520-  
767 0485\(1985\)015<0544:NIWPIG>2.0.CO;2](https://doi.org/10.1175/1520-0485(1985)015<0544:NIWPIG>2.0.CO;2)  
768
- 769 Lafuente, J. M. G., & Lucaya, N. C. (1994). Tidal dynamics and associated features of the  
770 northwestern shelf of the Alboran Sea. *Continental Shelf Research*, 14(1), 1-21.  
771 [https://doi.org/10.1016/0278-4343\(94\)90002-7](https://doi.org/10.1016/0278-4343(94)90002-7)  
772
- 773 Lie, H. J., Lee, S., & Cho, C. H. (2002). Computation methods of major tidal currents from  
774 satellite-tracked drifter positions, with application to the Yellow and East China Seas. *Journal of*  
775 *Geophysical Research: Oceans*, 107(C1), 3-1. <https://doi.org/10.1029/2001JC000898>  
776
- 777 Lilly, J. M., 2021, jLab: A data analysis package for Matlab, v.1.7.1,  
778 doi:10.5281/zenodo.4547006, <http://www.jmlilly.net/software>.  
779

780 Lozano, C. J., & Candela, J. (1995). The M (2) tide in the Mediterranean Sea: Dynamic analysis  
781 and data assimilation. *Oceanologica acta*, 18(4), 419-441.

782

783 Medvedev, I. P., Vilibić, I., & Rabinovich, A. B. (2020). Tidal resonance in the Adriatic Sea:  
784 Observational evidence. *Journal of Geophysical Research: Oceans*, 125(8), e2020JC016168.

785 <https://doi.org/10.1029/2020JC016168>

786

787 Menna, M., Poulain, P. M., Bussani, A., & Gerin, R. (2018). Detecting the drogue presence of  
788 SVP drifters from wind slippage in the Mediterranean Sea. *Measurement*, 125, 447-453.

789 <https://doi.org/10.1016/j.measurement.2018.05.022>

790

791 Millot, C., & Garcia-Lafuente, J. (2011). About the seasonal and fortnightly variabilities of the  
792 Mediterranean outflow. *Ocean Science*, 7(3), 421-428.

793 <https://doi.org/10.1016/j.measurement.2018.05.022>

794

795 Müller, M., Cherniawsky, J. Y., Foreman, M. G., & von Storch, J. S. (2014). Seasonal variation  
796 of the M 2 tide. *Ocean Dynamics*, 64, 159-177. <http://dx.doi.org/10.1007/s10236-013-0679-0>

797

798 Naranjo, C., Garcia-Lafuente, J., Sannino, G., & Sanchez-Garrido, J. C. (2014). How much do  
799 tides affect the circulation of the Mediterranean Sea? From local processes in the Strait of

800 Gibraltar to basin-scale effects. *Progress in Oceanography*, 127, 108-116.

801 <https://doi.org/10.1016/j.pocean.2014.06.005>

802

803 Pastusiak, T. (2020). Hydrology of tidal waters at the glacier terminus and their Impact on  
804 hydrographical surveys and navigation safety. *TransNav: International Journal on Marine*  
805 *Navigation and Safety of Sea Transportation*, 14(2). <http://dx.doi.org/10.12716/1001.14.02.21>

806

807 Pawlowicz, R., Beardsley, B., & Lentz, S. (2002). Classical tidal harmonic analysis including  
808 error estimates in MATLAB using T\_TIDE. *Computers & geosciences*, 28(8), 929-937.

809 [https://doi.org/10.1016/S0098-3004\(02\)00013-4](https://doi.org/10.1016/S0098-3004(02)00013-4)

810

811 Pawlowicz, R., 2020. "M\_Map: A mapping package for MATLAB", version 1.4m, [Computer  
812 software], available online at [www.eoas.ubc.ca/~rich/map.html](http://www.eoas.ubc.ca/~rich/map.html)

813

814 Percival, D. B., & Walden, A. T. (1993). *Spectral analysis for physical applications*. New York,  
815 Cambridge University Press.

816

817 Perkins, H. (1976, November). Observed effect of an eddy on inertial oscillations. In *Deep Sea*  
818 *Research and Oceanographic Abstracts* (Vol. 23, No. 11, pp. 1037–1042). Elsevier.

819 [http://doi.org/10.1016/0011-7471\(76\)90879-2](http://doi.org/10.1016/0011-7471(76)90879-2)

820

821 Poulain, P. M., & Zambianchi, E. (2007). Surface circulation in the central Mediterranean Sea as  
822 deduced from Lagrangian drifters in the 1990s. *Continental Shelf Research*, 27(7), 981-1001.

823 <https://doi.org/10.1016/j.csr.2007.01.005>

824

- 825 Poulain, P. M., Menna, M., & Mauri, E. (2012). Surface geostrophic circulation of the  
826 Mediterranean Sea derived from drifter and satellite altimeter data. *Journal of Physical*  
827 *Oceanography*, 42(6), 973-990. <https://doi.org/10.1175/JPO-D-11-0159.1>  
828
- 829 Poulain, P. M., Bussani, A., Gerin, R., Jungwirth, R., Mauri, E., Menna, M., & Notarstefano, G.  
830 (2013). Mediterranean surface currents measured with drifters: From basin to subinertial  
831 scales. *Oceanography*, 26(1), 38-47. <http://dx.doi.org/10.5670/oceanog.2013.03>  
832
- 833 Poulain, P. M., & Centurioni, L. (2015). Direct measurements of World Ocean tidal currents  
834 with surface drifters. *Journal of Geophysical Research: Oceans*, 120(10), 6986-7003.  
835 <https://doi.org/10.1002/2015JC010818>  
836
- 837 Poulain, P. M., Menna, M., & Gerin, R. (2018). Mapping Mediterranean tidal currents with  
838 surface drifters. *Deep Sea Research Part I: Oceanographic Research Papers*, 138, 22-33.  
839 <https://doi.org/10.1016/j.dsr.2018.07.011>  
840
- 841 Pugh, D.T. (1987). *Tides, surges and mean sea level*. New York, New York, John Wiley and  
842 Sons  
843
- 844 Ray, R. D. (2022). On seasonal variability of the M<sub>2</sub> tide. *Ocean Science*, 18(4), 1073–1079.  
845 <https://doi.org/10.5194/os-18-1073-2022>  
846

847 Rosentraub, Z., & Brenner, S. (2007). Circulation over the southeastern continental shelf and  
848 slope of the Mediterranean Sea: direct current measurements, winds, and numerical model  
849 simulations. *Journal of Geophysical Research: Oceans*, 112(C11).

850 <https://doi.org/10.1029/2006JC003775>

851

852 Sannino, G., Carillo, A., Pisacane, G., & Naranjo, C. (2015). On the relevance of tidal forcing in  
853 modelling the Mediterranean thermohaline circulation. *Progress in Oceanography*, 134, 304-

854 329. <https://doi.org/10.1016/j.pocean.2015.03.002>

855

856 Sammartino, S., García Lafuente, J., Naranjo, C., Sánchez Garrido, J. C., Sánchez Leal, R., &  
857 Sánchez Román, A. (2015). Ten years of marine current measurements in E spartel Sill, Strait of  
858 Gibraltar. *Journal of Geophysical Research: Oceans*, 120(9), 6309-6328.

859 <https://doi.org/10.1002/2014JC010674>

860

861 Shaffer, B. (2011). Israel—New natural gas producer in the Mediterranean. *Energy Policy*, 39(9),  
862 5379–5387. <https://doi.org/10.1016/j.enpol.2011.05.026>

863

864 Slepian, D. (1978). Prolate spheroidal wave functions, Fourier analysis, and uncertainty—V: The  
865 discrete case. *Bell System Technical Journal*, 5(5), 1371–1430. <https://doi.org/10.1002/j.1538->

866 7305.1978.tb02104.x

867

868 Soto-Navarro, J., Lorente, P., Alvarez Fanjul, E., Carlos Sánchez-Garrido, J., & García-Lafuente,  
869 J. (2016). Surface circulation at the Strait of Gibraltar: A combined HF radar and high resolution

870 model study. *Journal of Geophysical Research: Oceans*, 121(3), 2016-2034.

871 <https://doi.org/10.1002/2015JC011354>

872

873 Thomson, D. J. (1982). Spectrum estimation and harmonic analysis. *Proceedings of the*

874 *IEEE*, 70(9), 1055–1096. <https://doi.org/10.1109/PROC.1982.12433>

875

876 Thomson, R. E., & Emery, W. J. (2014). *Data analysis methods in physical oceanography*.

877 Newnes.

878

879 Tsimplis, M. N., Proctor, R., & Flather, R. A. (1995). A two-dimensional tidal model for the

880 Mediterranean Sea. *Journal of Geophysical Research: Oceans*, 100(C8), 16223–16239.

881 <https://doi.org/10.1029/95JC01671>

882

883 Tsimplis, M. N., & Bryden, H. L. (2000). Estimation of the transports through the Strait of

884 Gibraltar. *Deep Sea Research Part I: Oceanographic Research Papers*, 47(12), 2219–2242.

885 [https://doi.org/10.1016/S0967-0637\(00\)00024-8](https://doi.org/10.1016/S0967-0637(00)00024-8)

886

887 Ursella, L., Kovačević, V., & Gačić, M. (2014). Tidal variability of the motion in the Strait of

888 Otranto. *Ocean Science*, 10(1), 49-67. <https://doi.org/10.5194/os-10-49-2014>

889

890 Vilibić, I., Šepić, J., Dadić, V., & Mihanović, H. (2010). Fortnightly oscillations observed in the

891 Adriatic Sea. *Ocean dynamics*, 60, 57-63. <https://doi.org/10.1007/s10236-009-0241-2>

892

893 Wang, D., Pan, H., Jin, G., & Lv, X. (2020). Seasonal variation of the principal tidal constituents  
894 in the Bohai Sea. *Ocean Science*, 16(1), 1-14. <https://doi.org/10.5194/os-16-1-2020>

895

896 Zaron, E. D., & Ray, R. D. (2017). Using an altimeter-derived internal tide model to remove  
897 tides from in situ data. *Geophysical Research Letters*, 44(9), 4241–  
898 4245. <https://doi.org/10.1002/2017GL072950>